Nuclear Science and Techniques (2023) 34:119
https://doi.org/10.1007/s41365-023-01269-1

Constraining nuclear symmetry energy with the charge radii of mirror-pair nuclei

Rong An[1,2,3] · **Shuai Sun**[1] · **Li-Gang Cao**[1,2] · **Feng-Shou Zhang**[1,2,4]

Received: 23 February 2023 / Revised: 25 May 2023 / Accepted: 30 May 2023 / Published online: 21 August 2023

Abstract

The nuclear charge radius plays a vital role in determining the equation of state of isospin asymmetric nuclear matter. Based on the correlation between the differences in charge radii of mirror-partner nuclei and the slope parameter (L) of symmetry energy at the nuclear saturation density, an analysis of the calibrated slope parameter L was performed in finite nuclei. In this study, relativistic and nonrelativistic energy density functionals were employed to constrain the nuclear symmetry energy through the available databases of the mirror-pair nuclei ^{36}Ca–^{36}S, ^{38}Ca–^{38}Ar, and ^{54}Ni–^{54}Fe. The deduced nuclear symmetry energy was located in the range 29.89–31.85 MeV, and L of the symmetry energy essentially covered the range 22.50–51.55 MeV at the saturation density. Moreover, the extracted L_s at the sensitivity density $\rho_s = 0.10$ fm^{-3} was located in the interval range 30.52–39.76 MeV.

Keywords Symmetry energy · Charge radii · Mirror nuclei

1 Introduction

Precise knowledge of nuclear symmetry energy (NSE), which is characterized as a component of the equation of state (EoS) of isospin asymmetric nuclear matter, can provide access to various physical phenomena relevant to a broad range of density profiles and energy scales [1, 2]. NSE plays an important role in understanding the nuclear structure. Moreover, the behavior of NSE may affect the properties of neutron stars [3–5] and help to comprehend the supernova explosion mechanism and stellar nucleosynthesis in astrophysical studies [6].

The density dependence of NSE, that is, $E_s(\rho)$, can be expanded around the saturation density ρ_0 ($\simeq 0.16$ fm^{-3}) as follows:

$$E_s(\rho) \approx E_s(\rho_0) + \frac{L}{3}\left(\frac{\rho-\rho_0}{\rho_0}\right) + \frac{K_{sym}}{18}\left(\frac{\rho-\rho_0}{\rho_0}\right)^2 + \ldots, \quad (1)$$

where L and K_{sym} are the slope and curvature of the symmetry energy at the nuclear saturation density ρ_0, respectively. The symmetry energy is believed to be associated with the isovector-sensitive indicators in the EoS of isospin asymmetric systems. Unfortunately, a direct connection between the experimental observables and the EoS is not possible.

This work was partly supported by the Key Laboratory of High Precision Nuclear Spectroscopy, Institute of Modern Physics, Chinese Academy of Sciences, the National Natural Science Foundation of China (Nos. 12135004, 11635003, 11961141004, 12275025, and 11975096), and the Fundamental Research Funds for Central Universities (No. 2020NTST06).

✉ Li-Gang Cao
caolg@bnu.edu.cn

✉ Feng-Shou Zhang
fszhang@bnu.edu.cn

[1] Key Laboratory of Beam Technology of Ministry of Education, College of Nuclear Science and Technology, Beijing Normal University, Beijing 100875, China

[2] Key Laboratory of Beam Technology of Ministry of Education, Institute of Radiation Technology, Beijing Academy of Science and Technology, Beijing 100875, China

[3] CAS Key Laboratory of High Precision Nuclear Spectroscopy, Institute of Modern Physics, Chinese Academy of Sciences, Lanzhou 730000, China

[4] Center of Theoretical Nuclear Physics, National Laboratory of Heavy Ion Accelerator of Lanzhou, Lanzhou 730000, China

Consequently, the microscopic implications of NSE can be extracted indirectly from the ground and the collective excited state properties of atomic nuclei, reaction observables, and detected dense astrophysical events [7, 8].

Thus far, enormous efforts have been undertaken to determine the EoS over the spread of density profiles and energy scales [9]. The neutron skin thickness (NST) of a heavy nucleus provides an available constraint on the EoS of neutron-rich matter around ρ_0 [10–17]. In the laboratory, the radius of ^{208}Pb has been detected by measuring parity-violating asymmetry in polarized elastic electron scattering experiments, for example, sequentially in the PREX-II [18]. The accuracy of NST has been further updated from the latest performance, namely $R_{\rm skin}^{208} = 0.283\pm0.071$ fm. The behavior of $E_{\rm s}(\rho)$ is mostly governed by the slope of the symmetry energy, L. The correlation between $R_{\rm skin}^{208}$ and the slope parameter L leads to a value of $L = 106\pm37$ MeV [19]. In addition, NSE can also be investigated using the isotope binding energy difference [20, 21] and double-magic nuclei [22, 23].

Significant progress has been made in evaluating NSE from the collective excited state properties of finite nuclei, such as isobaric analog states [24], pygmy dipole resonance (PDR) [25], electric dipole polarizability [26], giant dipole resonance (GDR) [27], isovector giant quadrupole resonance (IVGQR) [28], and charge-exchange giant resonance [29–32]. The results for L extracted from PDR in ^{68}Ni and ^{132}Sn were constrained to be in the intervals 50.3–89.4 MeV and 29.0–82.0 MeV [25], respectively. The deduced slope parameter from the weighted average can cover the range $L = 64.8\pm15.7$ MeV. As suggested in Ref. [28], the slope parameter of the symmetry energy can be reduced to 37 ± 18 MeV by exploiting IVGQR energies.

Moreover, NSE offers a key requirement for our understanding of nuclear reactions under isospin diffusions and isotopic distributions [33–35]. Heavy-ion collisions (HICs) provide a sensitive probe to link the nuclear EoS, which depends on isovector potentials. In transport models, NSE is derived by simulating isospin-sensitive observables [36–40]. Hence, many simulation codes are desirable to determine the NSE [41–46]. More details about the transport simulations can be found in a recent study [47]. Meanwhile, new observations of compact stellar objects have provided plentiful data that help discern the EoS across saturation densities [48, 49]. The range of L can be deduced from the observation of dense object events, such as the production of gravitational waves from the neutron star merger GW170817 [50], resulting in $L = 11$–65 MeV.

The density dependence of symmetry energy is fairly uncertain, except for the bulk properties at the saturation density ρ_0. This challenges us in reducing the intrinsic uncertainties of the model from multiple aspects of the isovector components. As demonstrated in Refs. [51, 52], the difference in the root-mean-square (rms) charge radii of mirror-pair nuclei ($\Delta R_{\rm ch}$) obtained using Skyrme functionals provides an alternative opportunity for calibrating the density dependence of NSE.

A related linear correlation between $\Delta R_{\rm ch}$ and the slope parameter L has been established. In Ref. [53], the differences in the charge radii of the mirror-partner nuclei ^{36}Ca–^{36}S and ^{38}Ca–^{38}Ar were investigated with varied values of L. It is evident that the slope parameter lies in the range $L = 5$-70 MeV. The latest precise determination evaluated the correlation between the difference in charge radii of the mirror-partner nuclei ^{54}Ni–^{54}Fe and the slope parameter, which implied a range of $L = 21$–88 MeV [54]. The rms charge radii of the nuclei ^{54}Ni and ^{54}Fe were obtained using Skyrme energy density functionals (EDFs) and covariant density functional theories (CDFTs), respectively.

As demonstrated above, $\Delta R_{\rm ch}$ of mirror-pair nuclei can be employed to extract information about L. The latest results of the charge radii of ^{54}Ni can facilitate efficient exploration of the nuclear EoS. The experimental data for $R_{\rm ch}$ and $\Delta R_{\rm ch}$ of the corresponding mirror partners are listed in Table 1 [53–55]. The NSE characterized as an isovector indicator in effective interactions should be systematically evaluated based on the latest experiments. To further obtain a comprehensive conclusion about the correlations between L and $\Delta R_{\rm ch}$, $\Delta R_{\rm ch}$ for the pairs of mass numbers $A = 36$, 38, and 54 can be calculated using nonrelativistic and relativistic (covariant) EDFs. Although the correlations between the incompressibility coefficients and isovector parameters are generally weaker than the correlations between the slope parameter L and symmetry energy [56], the uncertainty suffered from nuclear incompressibility is inevitable in the evaluated process. Therefore, the values of incompressibility coefficients characterized as isoscalar parameters are almost identical for the two types of EDFs.

The remainder of this paper is organized as follows: in Sect. 2, we briefly report the theoretical models. In Sect. 3, we present the results and discussion. Finally, a summary and an outlook are provided in Sect. 4.

Table 1 $R_{\rm ch}$ and $\Delta R_{\rm ch}$ database for the $A = 36$, 38, and 54 mirror-pair nuclei. The parentheses beside the values of charge radii and the difference in charge radii are systematic uncertainties [53–55]

A		$R_{\rm ch}$ (fm)	$\Delta R_{\rm ch}$ (fm)
36	Ca	3.4484(27)	
	S	3.2982(12)	0.150(4)
38	Ca	3.4652(17)	
	Ar	3.4022(15)	0.063(3)
54	Ni	3.7370(30)	
	Fe	3.6880(17)	0.049(4)

2 Theoretical framework

In this study, we adopted two types of widely used nuclear density functionals to extract information about the nuclear matter EoS, namely the sophisticated Skyrme and covariant EDFs. Both have achieved great success in describing the bulk properties of finite nuclei, such as binding energies and charge radii. For a detailed introduction to nonrelativistic and relativistic EDFs, refer to Refs. [57–59]. In this paper, we briefly introduce the two nuclear density functionals. The effective interaction in sophisticated Skyrme-type EDFs, which is expressed as an effective zero-range force between nucleons with density-dependence and momentum-dependence terms, is as follows: [60, 61]

$$\begin{aligned} V(\mathbf{r}_1,\mathbf{r}_2) =& t_0(1+x_0\mathbf{P}_\sigma)\delta(\mathbf{r}) \\ &+\frac{1}{2}t_1(1+x_1\mathbf{P}_\sigma)\left[\mathbf{P}'^2\delta(\mathbf{r})+\delta(\mathbf{r})\mathbf{P}^2\right] \\ &+t_2(1+x_2\mathbf{P}_\sigma)\mathbf{P}'\cdot\delta(\mathbf{r})\mathbf{P} \\ &+\frac{1}{6}t_3(1+x_3\mathbf{P}_\sigma)[\rho(\mathbf{R})]^\alpha\delta(\mathbf{r}) \\ &+\mathrm{i}W_0\boldsymbol{\sigma}\cdot\left[\mathbf{P}'\times\delta(\mathbf{r})\mathbf{P}\right], \end{aligned} \tag{2}$$

where $\mathbf{r}=\mathbf{r}_1-\mathbf{r}_2$ and $\mathbf{R}=(\mathbf{r}_1+\mathbf{r}_2)/2$ are related to the positions of two nucleons, $\mathbf{P}=(\nabla_1-\nabla_2)/2\mathrm{i}$ is the relative momentum operator and $\mathbf{P}'$ is its complex conjugate acting on the left, $\sigma=\vec{\sigma}_1+\vec{\sigma}_2$, and $\mathbf{P}_\sigma=(1+\vec{\sigma}_1+\vec{\sigma}_2)/2$ is the spin exchange operator. The quantities α, t_i, and x_i (i = 0-3) represent the parameters of the Skyrme forces.

For covariant EDFs, the interacting Lagrangian density has the following form: [62, 63]

$$\begin{aligned} \mathcal{L} =& \bar{\psi}[\mathrm{i}\gamma^\mu\partial_\mu - M - g_\sigma\sigma - \gamma^\mu(g_\omega\omega_\mu + g_\rho\vec{\tau}\cdot\vec{\rho}_\mu + e\mathbf{A}_\mu)]\psi \\ &+\frac{1}{2}\partial^\mu\sigma\partial_\mu\sigma - \frac{1}{2}m_\sigma^2\sigma^2 - \frac{1}{3}g_2\sigma^3 - \frac{1}{4}g_3\sigma^4 \\ &-\frac{1}{4}\boldsymbol{\Omega}^{\mu\nu}\boldsymbol{\Omega}_{\mu\nu} + \frac{1}{2}m_\omega^2\omega_\mu\omega^\mu + \frac{1}{4}c_3(\omega^\mu\omega_\mu)^2 \\ &-\frac{1}{4}\vec{R}_{\mu\nu}\cdot\vec{R}^{\mu\nu} + \frac{1}{2}m_\rho^2\vec{\rho}^\mu\cdot\vec{\rho}_\mu \\ &+\Lambda_v(g_\rho^2\vec{\rho}_\mu\vec{\rho}^\mu)(g_\omega^2\omega_\mu\omega^\mu) - \frac{1}{4}\mathbf{F}^{\mu\nu}\mathbf{F}_{\mu\nu}. \end{aligned} \tag{3}$$

Here, $\boldsymbol{\Omega}_{\mu\nu}=\partial_\mu\omega_\nu-\partial_\nu\omega_\mu$, $\vec{R}_{\mu\nu}=\partial_\mu\vec{\rho}_\nu-\partial_\nu\vec{\rho}_\mu-g_\rho(\vec{\rho}_\mu\times\vec{\rho}_\nu)$, $\mathbf{F}_{\mu\nu}=\partial_\mu\mathbf{A}_\nu-\partial_\nu\mathbf{A}_\mu$, and M, m_σ, m_ω, and m_ρ are the nucleon, $\boldsymbol{\sigma}$, $\boldsymbol{\omega}$, and $\boldsymbol{\rho}$ meson masses, respectively. The quantities g_σ, g_ω, g_ρ, g_2, g_3, c_3, and $e^2/4\pi=1/137$ are the coupling constants for the $\boldsymbol{\sigma}$, $\boldsymbol{\omega}$, $\boldsymbol{\rho}$ mesons, and photons. The parameter set Λ_v represents the coupling strength between the ω and ρ mesons. Solving the Skyrme HF and Dirac equations on a spherical basis, one can obtain the eigenenergies and wave functions of the constituent nucleons, from which the bulk properties of the ground states can be obtained using this standard procedure [57–63].

In our applications, two families of parameter sets were adopted: the asy family for Skyrme EDFs [64] and the IUFSU family for covariant EDFs [65]. All of these effective forces were calibrated by fitting the parameters to specific observables of finite nuclei, such as binding energies and charge radii, and the isovector part of the EoS was generated in such a way that the symmetry energy remained at a fixed value (≈26 MeV) around a sensitivity baryon density of $\rho_s\approx 0.10$ fm^{-3}; thus, the interactions were characterized by different values of the symmetry energy at saturation density. This procedure ensures that the quality of the fit cannot be contaminated and that all isoscalar observables remain unchanged, for example, the incompressibility coefficient almost equals 230 MeV. In Fig. 1, the density dependence behaviors of the symmetry energies are plotted using the relativistic and Skyrme EDFs. With increasing symmetry energy at the saturation density $\rho_0\simeq 0.16$ fm^{-3}, the slope became larger for these two families of parameter sets. For the symmetry energy around the sensitivity density $\rho_s=0.10$ fm^{-3}, these values were almost unchanged. Further details can be found in Refs. [65, 66]. It is worth mentioning that both the symmetry energies and slope parameters can cover a wide range. To reduce the intrinsic uncertainties of the models, such parameterization sets should be expected to provide stringent constraints on observables that are

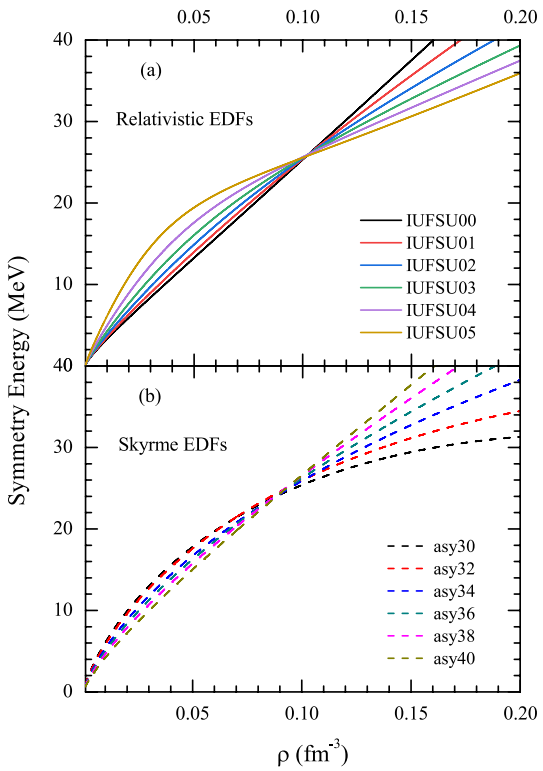

Fig. 1 (Color online) Symmetry energies characterized by relativistic EDFS (**a**) and Skyrme EDFs (**b**) plotted as a function of density

Table 2 Models used for the calculation of R_{ch}. The corresponding bulk properties of nuclear matter used in this study, such as symmetry energy E_s (MeV), the slope parameter L (MeV), and the incompressibility K_∞ (MeV) at saturation density, are given

Type	Sets	E_s (MeV)	L (MeV)	K_∞ (MeV)
RMF	IUFSU05	30.48	46.11	229.98
	IUFSU04	31.52	52.09	229.98
	IUFSU03	32.59	60.52	230.05
	IUFSU02	33.85	71.83	230.01
	IUFUS01	35.49	87.27	230.04
	IUFSU00	37.16	108.76	229.88
Skyrme	asy30	30.00	22.87	230.20
	asy32	31.99	36.22	229.99
	asy34	33.99	56.14	229.84
	asy36	36.00	71.54	229.93
	asy38	38.00	87.62	230.20
	asy40	40.01	106.09	230.09

highly sensitive to the density dependence of the symmetry energy. The corresponding values of the bulk properties of the nuclear matter are shown explicitly in Table 2.

3 Results and discussion

The results for ΔR_{ch} are plotted as functions of L in Fig. 2. The nonrelativistic Skyrme approach and RMF theory were used to assess the correlation between ΔR_{ch} and L, which are shown by the open circles and crosses in Fig. 2, respectively. The horizontal light blue bands indicate the uncertainties of ΔR_{ch}, which correspond to 0.146–0.154 fm (^{36}Ca–^{36}S), 0.060–0.066 fm (^{38}Ca–^{38}Ar), and 0.045–0.053 fm (^{54}Ni–^{54}Fe). The linear fits in the correction for ΔR_{ch} are indicated by the dashed lines.

The results obtained using the Skyrme and covariant EDFs revealed an approximate linear correlation between ΔR_{ch} and L. Constraints on L were deduced by comparing the theoretical predictions with the experimental results in Fig. 2. Note that the results for $A = 54$ provided the slope of symmetry energy L relevant to the range 17.99–62.43 MeV, whereas those for $A = 38$ and $A = 36$ were in the intervals 6.83–52.49 and 22.50-51.55 MeV, respectively. We can see that these values essentially cover the theoretical uncertainties in Refs. [53, 54].

The NST of ^{48}Ca is regarded as a feasible isovector indicator to constrain the EoS of nuclear matter. The high-resolution $E1$ polarizability experiment performed at RCNP suggests that the NST of ^{48}Ca is located in the interval 0.14 ∼ 0.20 fm [67]. Meanwhile, the CREX collaboration has reported a new value through parity-violating electron scattering measurements, namely 0.071 ∼ 0.171 fm [68]. The NST of ^{48}Ca allows a direct comparison to

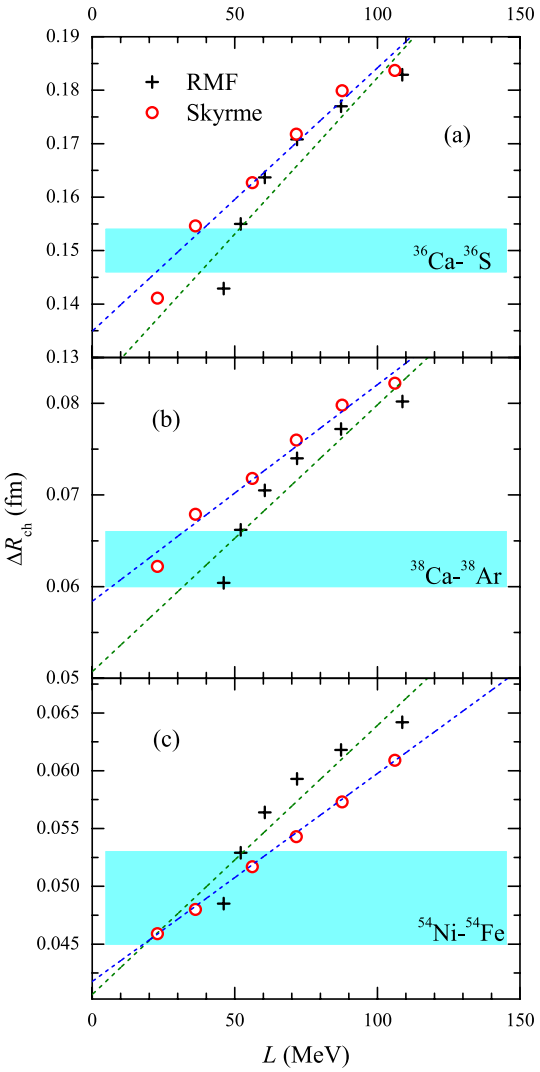

Fig. 2 (Color online) ΔR_{ch} of the mirror-partner nuclei ^{36}Ca–^{36}S (**a**), ^{38}Ca–^{38}Ar (**b**), and ^{54}Ni–^{54}Fe (**c**) as a function of the slope parameter L at the saturation density ρ_0. The experimental result is shown as a horizontal light blue band. The crosses are results of relativistic EDFs, and the open circles are for the Skyrme EDF calculations. The dashed lines indicate theoretical linear fits

microscopic calculations using various slope parameters, L. In Refs. [69, 70], the linear correlation analysis of ΔR_{ch} of mirror-partner nuclei and the corresponding NST has been clearly illustrated. Therefore, it is essential to evaluate the correlations between ΔR_{ch} of mirror-pair nuclei and the NST of ^{48}Ca.

The correlations between ΔR_{ch} of the $A = 36$, 38, and 54 mirror-partner nuclei and the NST of ^{48}Ca (ΔR_{np}) are also shown in Fig. 3. The calculated ΔR_{ch} substantially covered the current uncertainties of ΔR_{np}(^{48}Ca) for both types of EDFs. For the $A = 54$ mirror-pair nuclei, the Skyrme model gave a comparable correlation with respect to the RMF model. A high linear correlation between ΔR_{ch} of

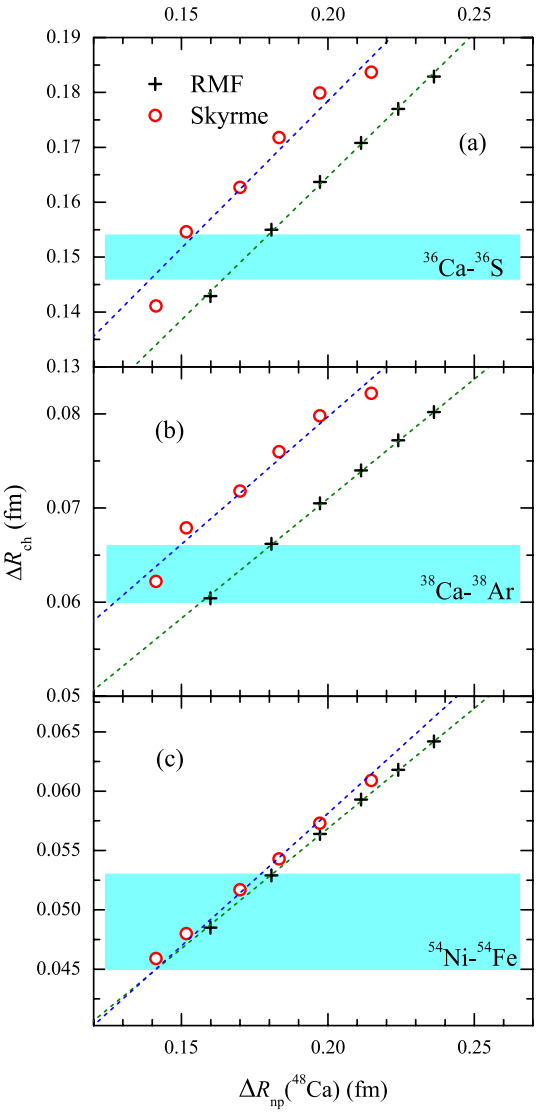

Fig. 3 (Color online) "Data-to-data" relation between ΔR_{ch} of the $A = 36$, 38, and 54 mirror-partner nuclei and the neutron skin thickness ΔR_{np} of ^{48}Ca. The labels and color coding are the same as those used in Fig. 2

$A = 54$ and ΔR_{np} of ^{48}Ca was found. These correlations were also obtained using nonrelativistic and relativistic EDFs for the $A = 36$ and 38 mirror partners, as shown in Figs. 3 a and b. This means that information on symmetry energy can be extracted from the differences in the charge radii of mirror-pair nuclei.

To obtain further constraints on the EoS of asymmetric nuclear matter, the relationship between the symmetry energy at saturation density and ΔR_{ch} of mirror-pair nuclei can also be evaluated as well as the relationship between L and ΔR_{ch}. Therefore, the "Data-to-data" relationships between the symmetry energies and the slope

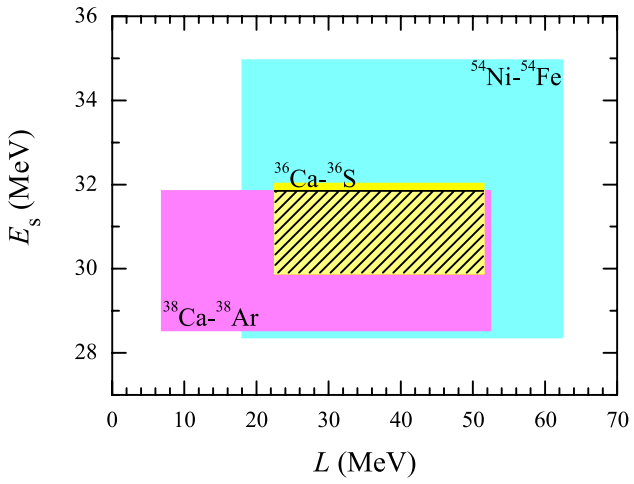

Fig. 4 (Color online) Symmetry energy E_s and the slope of symmetry energy L are limited by ΔR_{ch} of the $A = 36$ (yellow plane), 38 (light purple panel), and 54 (light blue plane) mirror-partner nuclei. The shadowed plane represents the result of the theoretical prediction in this study

parameters are shown in Fig. 4 via various colored planes for the $A = 36$ (Ca–S), 38 (Ca–Ar), and 54 (Ni–Fe) mirror-partner nuclei. The shadowed plane represents the result of the theoretical prediction. From this figure, it is noticeable that the deduced symmetry energy was located in the interval $E_s = 29.89$–31.85 MeV, and the slope of the symmetry energy covered the range $L = 22.50$–51.55 MeV. It should be mentioned that the present value provides a tighter constraint on L than those in Refs. [53, 54]. Although the mirror-partner nuclei for the masses $A = 36$, 38, and 54 were simultaneously considered in our evaluated procedure, the effects of deformation and model uncertainties were not incorporated in our calculations as in Refs. [53, 54]. In forthcoming investigations, we will carefully study the effect of deformation on the charge radius of finite nuclei and estimate the model uncertainties using a comprehensive set of modern density functionals, which may change the present results.

To facilitate the quantitative comparison of the extracted results with the theoretical calculations, various available estimates of the slope parameter L of the symmetry energy are shown in Fig. 5. It is evident that our present result has a remarkable overlap with the results obtained by various methods or observables. Our calculations predominantly covered the result for L extracted from PDR in ^{132}Sn ($L = 29.0$–82.0 MeV) but deviated from that of ^{68}Ni ($L = 50.3$–89.4 MeV) [25]. Figure 5 shows the weighted average value in the interval of 64.8 ± 15.7 MeV. In addition, the electric dipole polarizability of a heavy nucleus is highly sensitive to both the magnitude and slope parameter of symmetry energy, providing a value of $L = 47.3 \pm 7.8$ MeV [26]. By exploiting this correlation together with

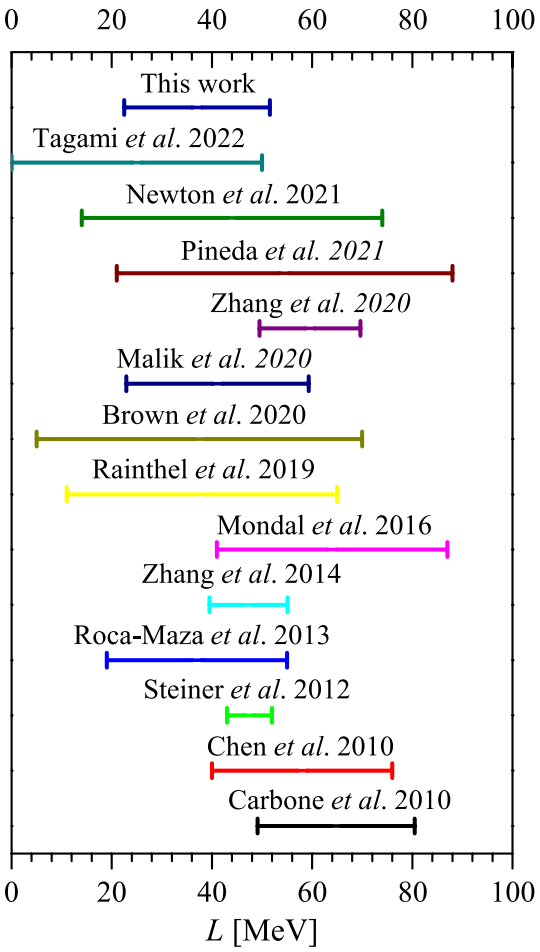

Fig. 5 (Color online) Comparison between the values of L extracted in this study and those from existing literature. We partly compare the values extracted from various models: Carbone *et al.* [25], Chen *et al.* [71], Steiner *et al.* [75], Roca-Maza *et al.* [28], Zhang *et al* [26], Mondal *et al.* [13], Raithel *et al.* [50], Brown *et al.* [53], Malik *et al.* [76], Zhang *et al.* [74], Pineda *et al.* [54], Newton *et al.* [80], and Tagami, *et al.* [72]

the experimental values of the isoscalar and isovector giant quadrupole resonance (GQR) energies, the slope parameter of the symmetry energy was estimated as $L = 37 \pm 18$ MeV [28]. Both theoretical results essentially covered the current uncertainty in this study.

The NST $\Delta r_{\rm np}$ in heavy nuclei provides an alternative terrestrial probe to place restrictions on the nuclear EoS. In Ref. [71], an accuracy value of $L = 58 \pm 18$ MeV was deduced by analyzing the neutron skin data on Sn isotopes and the observables originating from HICs. Our calibrated results covered the uncertainty of this value. The latest NST of ^{48}Ca detected by the CREX group yielded the slope parameter $L = 0 \sim 50$ MeV [72], which is in accordance with this study ($L = 22.50$-51.55 MeV). Significantly, the NST of ^{208}Pb detected by the PREX-II group yielded a larger value of $L = 76 \sim 165$ MeV. Reed et al. [19] reported a comparable interval of the slope parameter $L = 106 \pm 37$ MeV. These values partially cover the interval range of $L = 54 \sim 97$ MeV induced by HICs [73]. However, the evaluated range in this literature has no overlap with the slope parameter L obtained by PREX-II.

In Ref. [74], more information, such as heavy-ion collision data, the neutron skin of ^{208}Pb, tidal deformability, and the maximum mass of neutron dense objects, was used to calibrate the values of symmetry energy. This led to a symmetry energy slope of $L = 59.57 \pm 10.06$ MeV, and the quantitative uncertainty was further reduced with respect to Ref. [71]. Moreover, the slope parameter L can be constrained by various observed astrophysical messages, except in terrestrial nuclear experiments. The currently available neutron star mass and radius measurements provide an important constraint on the EoS of neutron matter through quantum Monte Carlo simulations, in which the slope parameter L is located in the range 43–52 MeV [75]. The correlation of the tidal deformability of a neutron star with L was studied using the skΛ267 model, which gave the range $L = 41.1 \pm 18.2$ MeV [76]. Moreover, the range $L = 11$–65 MeV was extracted from the observation of a gravitational-wave event of the neutron star merger GW170817 [50]. Our calibrated range ($L = 22.50$–51.55 MeV) overlaps significantly with these deduced values.

Recently, emerging Bayesian frameworks have been developed widely to study the bulk properties of finite nuclei, for example, predictions in the nuclear charge radii [77, 78] and nuclear EoSs [79]. The existing database of neutron skin and the bulk properties of nuclear matter are characterized by prior input quantities, which leads to credible values of $L = 40^{+34}_{-26}$ MeV and $L = 37^{+9}_{-8}$ MeV [80], respectively. All the evaluated values are consistent with the range of L obtained in this study.

As mentioned in Refs. [81, 82], the density dependence of the symmetry energy at the subsaturation density is associated with nuclear mass differences and multifragmentation production. Thus, it is also interesting to give the constraint of the slope parameter $L_{\rm s}$ at the sensitivity density $\rho_{\rm s} = 0.10$ fm^{-3} probed by the differences in the charge radii of mirror-partner nuclei ($\Delta R_{\rm ch}$). In Fig. 6, $\Delta R_{\rm ch}$ of the mirror-partner nuclei ^{36}Ca–^{36}S (a), ^{38}Ca–^{38}Ar (b), and ^{54}Ni–^{54}Fe (c) as a function of the slope parameter $L_{\rm s}$ at the sensitivity density $\rho_{\rm s} = 0.10$ fm^{-3} are plotted. The highly linear correlations between $\Delta R_{\rm ch}$ and L_s are also presented. The extracted interval range of the slope parameter $L_{\rm s}$ at the sensitivity density $\rho_{\rm s} = 0.10$ fm^{-3} was approximately 30.52–39.76 MeV. This restricted value is relatively narrow compared to the interval range at the saturation density $\rho_0 \simeq 0.16$ fm^{-3}.

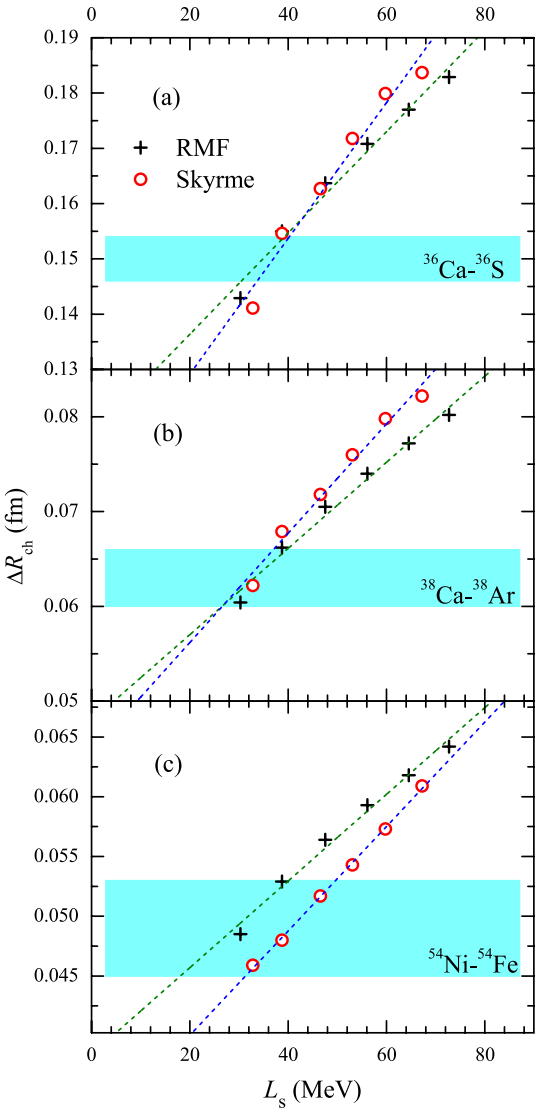

Fig. 6 (Color online) Same as Fig. 2, but for the slope parameter L_s at the sensitivity density $\rho_s = 0.10$ fm^{-3}

4 Summary and outlook

Microscopic methods based on families of nonrelativistic and relativistic EDFs were employed to characterize a systematic variation of the isoscalar and isovector properties of corresponding nuclear matter EoSs. Our systematic analysis of the extraction of the slope parameter L from the differences in mirror-partner nuclei charge radii provided a new result. The slope parameter L covered the interval range 22.50–51.55 MeV at the saturation density. Moreover, the slope parameter L_s at the sensitivity density $\rho_s = 0.10$ fm^{-3} lay in the interval range 30.52–39.76 MeV. This led to us determining the density dependence of symmetry energy relatively accurately, which is a fundamental quantity for nuclear physics and for the implications in the study of neutron stars.

Linear fits were performed between the differences in the charge radii of mirror-partner nuclei and the slope parameter L. As suggested in Refs. [83–87], precise descriptions of the nuclear charge radii are influenced by various mechanisms. Meanwhile, the precise measurement of the charge density distributions usually affects the NST of finite nuclei on a quantitative level. In Ref. [88], it is demonstrated that the differences in the charge radii of mirror-pair nuclei are systematically influenced by the pairing correlations. For weakly bound nuclei, configuration mixing should be discreetly considered when tackling pairing correlations [89]. Hence, this study should be further reviewed.

Author Contributions All authors contributed to the study conception and design. Material preparation, data collection, and analysis were performed by Rong An, Shuai Sun, Li-Gang Cao, and Feng-Shou Zhang. The first draft of the manuscript was written by Rong An and all authors commented on previous versions of the manuscript. All authors read and approved the final manuscript.

Declarations

Conflict of interest Feng-Shou Zhang is an editorial board member for Nuclear Science and Techniques and was not involved in the editorial review, or the decision to publish this article. All authors declare that there are no competing interests.

References

1. A.W. Steiner, M. Prakash, J.M. Lattimer et al., Isospin asymmetry in nuclei and neutron stars. Phys. Rept. **411**, 325 (2005). https://doi.org/10.1016/j.physrep.2005.02.004
2. B.-A. Li, L.-W. Chen, C.M. Ko, Recent progress and new challenges in isospin physics with heavy ion reactions. Phys. Rept. **464**, 113 (2008). https://doi.org/10.1016/j.physrep.2008.04.005
3. F. Ji, J.N. Hu, S.S. Bao et al., Effects of nuclear symmetry energy and equation of state on neutron star properties. Phys. Rev. C **100**, 045801 (2019). https://doi.org/10.1103/PhysRevC.100.045801
4. Z. Qian, R.Y. Xin, B.Y. Sun, Moments of inertia of neutron stars in relativistic mean field theory: the role of the isovector scalar channel. Sci. China-Phys. Mech. Astron. **61**, 082011 (2018). https://doi.org/10.1007/s11433-018-9182-3
5. J.F. Xu, C.J. Xia, Z.Y. Lu et al., Symmetry energy of strange quark matter and tidal deformability of strange quark stars. Nucl. Sci. Tech. **33**, 143 (2022). https://doi.org/10.1007/s41365-022-01130-x
6. J.M. Lattimer, M. Prakash, Neutron star observations: prognosis for equation of state constraints. Phys. Rept. **442**, 109 (2007). https://doi.org/10.1016/j.physrep.2007.02.003
7. M. Baldo, G. Burgio, The nuclear symmetry energy. Prog. Part. Nucl. Phys. **91**, 203 (2016). https://doi.org/10.1016/j.ppnp.2016.06.006
8. X. Roca-Maza, N. Paar, Nuclear equation of state from ground and collective excited state properties of nuclei. Prog. Part. Nucl. Phys. **101**, 96 (2018). https://doi.org/10.1016/j.ppnp.2018.04.001
9. M.B. Tsang, J.R. Stone, F. Camera et al., Constraints on the symmetry energy and neutron skins from experiments and

theory. Phys. Rev. C **86**, 015803 (2012). https://doi.org/10.1103/PhysRevC.86.015803
10. M. Centelles, X. Roca-Maza, X. viñas, et al., Nuclear symmetry energy probed by neutron skin thickness of nuclei. Phys. Rev. Lett. **102**, 122502 (2009). https://doi.org/10.1103/PhysRevLett.102.122502
11. P.-G. Reinhard, W. Nazarewicz, Information content of a new observed: the case of the nuclear neutron skin. Phys. Rev. C **81**, 051303(R) (2010). https://doi.org/10.1103/PhysRevC.81.051303
12. Z. Zhang, L.-W. Chen, Constraining symmetry energy at subsaturation densities using isotope binding energy difference and neutron skin thickness. Phys. Lett. B **726**, 234 (2013). https://doi.org/10.1016/j.physletb.2013.08.002
13. C. Mondal, B.K. Agrawal, M. Centelles et al., Model dependence of the neutron-skin thickness on the symmetry energy. Phys. Rev. C **93**, 064303 (2016). https://doi.org/10.1103/PhysRevC.93.064303
14. M. Liu, Z.-X. Li, N. Wang et al., Exploring nuclear symmetry energy with isospin dependence on neutron skin thickness of nuclei. Chin. Phys. C **35**, 629 (2011). https://doi.org/10.1088/1674-1137/35/7/006
15. X.-H. Fan, J.-M. Dong, W. Zuo, Symmetry energy at subsaturation densities and neutron skin thickness of ^{208}Pb. Sci. China-Phys. Mech. Astron. **58**, 062002 (2015). https://doi.org/10.1007/s11433-015-5673-8
16. C. Xu, Z.-Z. Ren, J. Liu, Attempt to link the neutron skin thickness of ^{208}Pb with the symmetry energy through cluster radioactivity. Phys. Rev. C **90**, 064310 (2014). https://doi.org/10.1103/PhysRevC.90.064310
17. J. Xu, W.-J. Xie, B.-A. Li, Bayesian inference of nuclear symmetry energy from measured and imagined neutron skin thicknesses in ^{116,118,120,122,124,130,132} Sn ,^{208} Pb, and ^{48} Ca. Phys. Rev. C **102**, 044316 (2020). https://doi.org/10.1103/PhysRevC.102.044316
18. D. Adhikari, H. Albataineh, D. Androic et al., (PREX Collaboration), Accurate determination of the neutron skin thickness of ^{208} Pb through parity-violation in electron scattering. Phys. Rev. Lett. **126**, 172502 (2021). https://doi.org/10.1103/PhysRevLett.126.172502
19. B.T. Reed, F.J. Fattoyev, C.J. Horowitz et al., Implications of PREX-2 on the equation of state of neutron-rich matter. Phys. Rev. Lett. **126**, 172503 (2021). https://doi.org/10.1103/PhysRevLett.126.172503
20. P. Danielewicz, Surface symmetry energy. Nucl. Phys. A **727**, 233 (2003). https://doi.org/10.1016/j.nuclphysa.2003.08.001
21. M. Liu, N. Wang, Z.-X. Li et al., Nuclear symmetry energy at subnormal densities from measured nuclear masses. Phys. Rev. C **82**, 064306 (2010). https://doi.org/10.1103/PhysRevC.82.064306
22. B.A. Brown, Constraints on the Skyrme equations of state from properties of doubly magic nuclei. Phys. Rev. Lett. **111**, 232502 (2013). https://doi.org/10.1103/PhysRevLett.111.232502
23. N. Wan, C. Xu, Z.-Z. Ren, Density slope of symmetry energy $L(\rho_0)$ constrained by proton radioactivity. Phys. Rev. C **94**, 044322 (2016). https://doi.org/10.1103/PhysRevC.94.044322
24. P. Danielewicz, J. Lee, Symmetry energy II: isobaric analog states. Nucl. Phys. A **922**, 1 (2014). https://doi.org/10.1016/j.nuclphysa.2013.11.005
25. A. Carbone, G. Colò, A. Bracco et al., Constraints on the symmetry energy and neutron skins from pygmy resonances in ^{68} Ni and ^{132} Sn. Phys. Rev. C **81**, 041301 (2010). https://doi.org/10.1103/PhysRevC.81.041301
26. Z. Zhang, L.-W. Chen, Constraining the density slope of the nuclear symmetry energy at subsaturation densities using the electric dipole polarizability in ^{208} Pb. Phys. Rev. C **90**, 064317 (2014). https://doi.org/10.1103/PhysRevC.90.064317
27. L.-G. Cao, Z.-Y. Ma, Symmetric energy and isovector giant dipole resonance in finite nuclei. Chin. Phys. Lett. **25**, 1625 (2008). https://doi.org/10.1088/0256-307X/25/5/028
28. X. Roca-Maza, M. Brenna, B.K. Agrawal et al., Giant quadrupole resonances in ^{208}Pb, the nuclear symmetry energy, and the neutron skin thickness. Phys. Rev. C **87**, 034301 (2013). https://doi.org/10.1103/PhysRevC.87.034301
29. L.-G. Cao, X. Roca-Maza, G. Colò et al., Constraints on the neutron skin and symmetry energy from the anti-analog giant dipole resonance in ^{208} Pb. Phys. Rev. C **92**, 034308 (2015). https://doi.org/10.1103/PhysRevC.92.034308
30. X. Roca-Maza, L.-G. Cao, G. Col;o, et al., Fully self-consistent study of charge-exchange resonances and their impact on symmetry energy parameters. Phys. Rev. C **94**, 044313 (2016). https://doi.org/10.1103/PhysRevC.94.044313
31. A. Krasznahorkay, N. Paar, D. Vretenar et al., Anti-analog giant dipole resonances and the neutron skin of nuclei. Phys. Lett. B **720**, 428 (2013). https://doi.org/10.1016/j.physletb.2013.02.043
32. S.-H. Cheng, J. Wen, L.-G. Cao et al., Neutron skin thickness of ^{90}Zr and symmetry energy constrained by charge exchange spin-dipole excitations. Chin. Phys. C **47**, 024102 (2023). https://doi.org/10.1088/1674-1137/aca38e
33. M. Colonna, V. Baran, M. Di Toro, Theoretical predictions of experimental observables sensitive to the symmetry energy. Eur. Phys. J. A **50**, 30 (2014). https://doi.org/10.1140/epja/i2014-14030-1
34. M. Colonna, Fluctuations and symmetry energy in nuclear fragmentation dynamics. Phys. Rev. Lett. **110**, 042701 (2013). https://doi.org/10.1103/PhysRevLett.110.042701
35. G.-F. Wei, X. Huang, Q.-J. Zhi et al., Effects of momentum dependence of nuclear symmetry potential on pion observables in Sn + Sn collisions at 270 MeV/nucleon. Nucl. Sci. Tech. **33**, 163 (2022). https://doi.org/10.1007/s41365-022-01146-3
36. Y.J. Wang, C.C. Guo, Q.F. Li et al., The effect of symmetry potential on the balance energy of light particles emitted from mass symmetric heavy-ion collisions with isotopes, isobars and isotones. Sci. China-Phys. Mech. Astron. **55**, 2407–2413 (2012). https://doi.org/10.1007/s11433-012-4922-3
37. A. Ono, J. Xu, M. Colonna et al., Comparison of heavy-ion transport simulations: collision integral with pions and Δ resonances in a box. Phys. Rev. C **100**, 044617 (2019). https://doi.org/10.1103/PhysRevC.100.044617
38. G. Jhang, J. Estee, J. Barney et al., Symmetry energy investigation with pion production from Sn+Sn systems. Phys. Lett. B **813**, 136016 (2021). https://doi.org/10.1016/j.physletb.2020.136016
39. J. Estee, W.G. Lynch, C.Y. Tsang et al., (SπRIT Collaboration), Probing the symmetry energy with the spectral pion ratio. Phys. Rev. Lett. **126**, 162701 (2021). https://doi.org/10.1103/PhysRevLett.126.162701
40. M.B. Tsang, Y. Zhang, P. Danielewicz et al., Constraints on the density dependence of the symmetry energy. Phys. Rev. Lett. **102**, 122701 (2009). https://doi.org/10.1103/PhysRevLett.102.122701
41. Z.-Q. Feng, G.-M. Jin, Probing high-density behavior of symmetry energy from pion emission in heavy-ion collisions. Phys. Lett. B **683**, 140 (2010). https://doi.org/10.1016/j.physletb.2009.12.006
42. M.A. Famiano, T. Liu, W.G. Lynch et al., Neutron and proton transverse emission ratio measurements and the density dependence of the asymmetry term of the nuclear equation of state. Phys. Rev. Lett. **97**, 052701 (2006). https://doi.org/10.1103/PhysRevLett.97.052701
43. W.-J. Xie, J. Su, L. Zhu et al., Symmetry energy and pion production in the Boltzmann-Langevin approach. Phys. Lett. B **718**, 1510 (2013). https://doi.org/10.1016/j.physletb.2012.12.021

44. W.-J. Xie, F.-S. Zhang, Nuclear collective flows as a probe for neutron-proton effective mass splitting. Phys. Lett. B **735**, 250 (2014). https://doi.org/10.1016/j.physletb.2014.06.050
45. H. Yu, D.-Q. Fang, Y.-G. Ma, Investigation of the symmetry energy of nuclear matter using isospin-dependent quantum molecular dynamics. Nucl. Sci. Tech. **31**, 61 (2020). https://doi.org/10.1007/s41365-020-00766-x
46. W.D. Tian, Y.-G. Ma, X.Z. Cai et al., Isospin and symmetry energy study in nuclear EOS. Sci. China-Phys. Mech. Astron **54**, 141–148 (2011). https://doi.org/10.1007/s11433-011-4424-8
47. M. Colonna, Y.-X. Zhang, Y.-J. Wang et al., Comparison of heavy-ion transport simulations: mean-field dynamics in a box. Phys. Rev. C **104**, 024603 (2021). https://doi.org/10.1103/PhysRevC.104.024603
48. M.C. Miller, F.K. Lamb, A.J. Dittmann et al., PSR J0030+0451 mass and radius from NICER data and implications for the properties of neutron star matter. Astrophys. J. **887**, L24 (2019). https://doi.org/10.3847/2041-8213/ab50c5
49. G. Raaijmakers, S.K. Greif, K. Hebeler et al., Constraints on the dense matter equation of state and neutron star properties from NICER's mass-radius estimate of PSR J0740+6620 and multimessenger observations. Astrophys. J. Lett. **918**, L29 (2021). https://doi.org/10.3847/2041-8213/ac089a
50. C.A. Raithel, F. Özel, Measurement of the nuclear symmetry energy parameters from gravitational-wave events. Astrophys. J. **885**, 121 (2019). https://doi.org/10.3847/1538-4357/ab48e6
51. N. Wang, T. Li, Shell and isospin effects in nuclear charge radii. Phys. Rev. C **88**, 011301(R) (2013). https://doi.org/10.1103/PhysRevC.88.011301
52. B.A. Brown, Mirror charge radii and the neutron equation of state. Phys. Rev. Lett. **119**, 122502 (2017). https://doi.org/10.1103/PhysRevLett.119.122502
53. B.A. Brown, K. Minamisono, J. Piekarewicz et al., Implications of the ^{36} Ca $-^{36}$ S and ^{38} Ca $-^{38}$ Ar difference in mirror charge radii on the neutron matter equation of state. Phys. Rev. Res. **2**, 022035 (2020). https://doi.org/10.1103/PhysRevResearch.2.022035
54. S.V. Pineda, K. König, D.M. Rossi et al., Charge radius of neutron-deficient ^{54} Ni and symmetry energy constraints using the difference in mirror pair charge radii. Phys. Rev. Lett. **127**, 182503 (2021). https://doi.org/10.1103/PhysRevLett.127.182503
55. A.J. Miller, K. Minamisono, A. Klose et al., Proton superfluidity and charge radii in proton-rich calcium isotopes. Nat. Phys. **15**, 432 (2019). https://doi.org/10.1038/s41567-019-0416-9
56. J. Xu, Z. Zhang, B.-A. Li, Uncertainty quantification for nuclear matter incompressibility. Phys. Rev. C **104**, 054324 (2021). https://doi.org/10.1103/PhysRevC.104.054324
57. M. Bender, P.-H. Heenen, P.-G. Reinhard, Self-consistent mean-field models for nuclear structure. Rev. Mod. Phys. **75**, 121 (2003). https://doi.org/10.1103/RevModPhys.75.121
58. D. Vretenar, A. Afanasjev, G. Lalazissis et al., Relativistic Hartree-Bogoliubov theory: static and dynamic aspects of exotic nuclear structure. Phys. Rep. **409**, 101 (2005). https://doi.org/10.1016/j.physrep.2004.10.001
59. H. Liang, J. Meng, S.-G. Zhou, Hidden pseudospin and spin symmetries and their origins in atomic nuclei. Phys. Rep. **570**, 1 (2015). https://doi.org/10.1016/j.physrep.2014.12.005
60. E. Chabanat, P. Bonche, P. Haensel et al., A Skyrme parametrization from subnuclear to neutron star densities. Nucl. Phys. A **627**, 710 (1997). https://doi.org/10.1016/S0375-9474(97)00596-4
61. E. Chabanat, P. Bonche, P. Haensel et al., A Skyrme parametrization from subnuclear to neutron star densities Part II Nuclei far from stabilities. Nucl. Phys. A **635**, 231 (1998). https://doi.org/10.1016/S0375-9474(98)00180-8
62. C.J. Horowitz, J. Piekarewicz, Neutron star structure and the neutron radius of ^{208}Pb. Phys. Rev. Lett. **86**, 5647 (2001). https://doi.org/10.1103/PhysRevLett.86.5647
63. C.J. Horowitz, J. Piekarewicz, Neutron radii of ^{208} Pb and neutron stars. Phys. Rev. C **64**, 062802(R) (2001). https://doi.org/10.1103/PhysRevC.64.062802
64. G. Colò, (private communication)
65. J. Piekarewicz, Pygmy resonances and neutron skins. Phys. Rev. C **83**, 034319 (2011). https://doi.org/10.1103/PhysRevC.83.034319
66. G. Colò, N. Van Giai, J. Meyer et al., Microscopic determination of the nuclear incompressibility within the nonrelativistic framework. Phys. Rev. C **70**, 024307 (2004). https://doi.org/10.1103/PhysRevC.70.024307
67. D. Adhikari, H. Albataineh, D. Androic et al., Electric dipole polarizability of ^{48} Ca and implications for the neutron skin. Phys. Rev. Lett. **118**, 252501 (2017). https://doi.org/10.1103/PhysRevLett.118.252501
68. J. Birkhan, M. Miorelli, S. Bacca et al., (CREX Collaboration), Precision determination of the neutral weak form factor of ^{48} Ca. Phys. Rev. Lett. **129**, 042501 (2022). https://doi.org/10.1103/PhysRevLett.129.042501
69. M.K. Gaidarov, I. Moumene, A.N. Antonov et al., Proton and neutron skins and symmetry energy of mirror nuclei. Nucl. Phys. A **1004**, 122061 (2020). https://doi.org/10.1016/j.nuclphysa.2020.122061
70. F. Sammarruca, Proton skins, neutron skins, and proton radii of mirror nuclei. Front. Phys. **6**, 90 (2018). https://doi.org/10.3389/fphy.2018.00090
71. L.-W. Chen, C.M. Co, B.-A. Li et al., Density slope of nuclear symmetry energy from neutron skin thickness of heavy nuclei. Phys. Rev. C **82**, 024321 (2010). https://doi.org/10.1103/PhysRevC.82.024321
72. S. Tagami, T. Wakasa, M. Yahiro, Slope parameters determined from CREX and PREX2. Res. Phys. **43**, 106037 (2022). https://doi.org/10.1016/j.rinp.2022.106037
73. Y.-Y. Liu, Y.-J. Wang, Y. Cui et al., Insights into the pion production mechanism and symmetry energy at high density. Phys. Rev. C **103**, 014616 (2021). https://doi.org/10.1103/PhysRevC.103.014616
74. Y.-X. Zhang, M. Liu, C.-J. Xia et al., Constraints on symmetry energy and its associated parameters from nuclei to neutron stars. Phys. Rev. C **101**, 034303 (2020). https://doi.org/10.1103/PhysRevC.101.034303
75. A.W. Steiner, S. Gandolfi, Connecting neutron star observations to three-body forces in neutron matter and to the nuclear symmetry energy. Phys. Rev. Lett. **108**, 081102 (2012). https://doi.org/10.1103/PhysRevLett.108.081102
76. T. Malik, B.K. Agrawal, C. Providência et al., Unveiling the correlations of tidal deformability with the nuclear symmetry energy parameters. Phys. Rev. C **102**, 052801 (2020). https://doi.org/10.1103/PhysRevC.102.052801
77. X.-X. Dong, R. An, J.-X. Lu et al., Nuclear charge radii in Bayesian neural networks revisited. Phys. Lett. B **838**, 137726 (2023). https://doi.org/10.1016/j.physletb.2023.137726
78. X.-X. Dong, R. An, J.-X. Lu et al., Novel Bayesian neural network-based approach for nuclear charge radii. Phys. Rev. C **105**, 014308 (2022). https://doi.org/10.1103/PhysRevC.105.014308
79. W.-J. Xie, B.-A. Li, Bayesian inference of high-density nuclear symmetry energy from the radii of canonical neutron stars. Astrophys. J. **883**, 174 (2019). https://doi.org/10.3847/1538-4357/ab3f37
80. W.G. Newton, G. Crocombe, Nuclear symmetry energy from neutron skins and pure neutron matter in a Bayesian framework. Phys.

Rev. C **103**, 064323 (2021). https://doi.org/10.1103/PhysRevC.103.064323
81. X.-H. Fan, J.-M. Dong, W. Zuo, Density-dependent symmetry energy at subsaturation densities from nuclear mass differences. Phys. Rev. C **89**, 017305 (2014). https://doi.org/10.1103/PhysRevC.89.017305
82. S. Kumar, Y.G. Ma, G.Q. Zhang et al., Probing the density dependence of the symmetry energy via multifragmentation at subsaturation densities. Phys. Rev. C **84**, 044620 (2011). https://doi.org/10.1103/PhysRevC.84.044620
83. R. An, S.-S. Zhang, Charge radii of potassium isotopes in the RMF (BCS)* approach. Chin. Phys. C **46**, 054101 (2022). https://doi.org/10.1088/1674-1137/ac4b5c
84. R. An, X. Jiang, L.-G. Cao et al., Odd-even staggering and shell effects of charge radii for nuclei with even Z from 36 to 38 and from 52 to 62. Phys. Rev. C **105**, 014325 (2022). https://doi.org/10.1103/PhysRevC.105.014325
85. P.-G. Reinhard, W. Nazarewicz, R.F. Garcia Ruiz, Beyond the charge radius: The information content of the fourth radial moment. Phys. Rev. C **101**, 021301 (2020). https://doi.org/10.1103/PhysRevC.101.021301
86. P.-G. Reinhard, W. Nazarewicz, Nuclear charge densities in spherical and deformed nuclei: toward precise calculations of charge radii. Phys. Rev. C **103**, 054310 (2021). https://doi.org/10.1103/PhysRevC.103.054310
87. R. An, L.-S. Geng, S.-S. Zhang, Novel ansatz for charge radii in density functional theory. Phys. Rev. C **102**, 024307 (2020). https://doi.org/10.1103/PhysRevC.102.024307
88. P.-G. Reinhard, W. Nazarewicz, Information content of the differences in the charge radii of mirror nuclei. Phys. Rev. C **105**, L021301 (2022). https://doi.org/10.1103/PhysRevC.105.L021301
89. R. An, L.-S. Geng, S.-S. Zhang et al., Particle number conserving BCS approach in the relativistic mean field model and its application to $^{32-74}$Ca. Chin. Phys. C **42**, 114101 (2018). https://doi.org/10.1088/1674-1137/42/11/114101